Praise Worthy Prize

International Review of Electrical Engineering (I.R.E.E.), Vol. 5, N. 2
March-April 2010

Modeling, Control and Simulation of Full-Power Converter Wind Turbines Equipped with Permanent Magnet Synchronous Generator

R. Melício[1], V. M. F. Mendes[2], J. P. S. Catalão[1]

Abstract – *In this paper, two wind turbines equipped with a permanent magnet synchronous generator (PMSG) and respectively with a two-level or a multilevel converter are simulated in order to access the malfunction transient performance. Three different drive train mass models, respectively, one, two and three mass models, are considered in order to model the bending flexibility of the blades. Moreover, a fractional-order control strategy is studied comparatively to a classical integer-order control strategy. Computer simulations are carried out, and conclusions about the total harmonic distortion (THD) of the electric current injected into the electric grid are in favor of the fractional-order control strategy.* ***Copyright © 2010 Praise Worthy Prize S.r.l. - All rights reserved.***

Keywords: *Fractional-Order Controller, Pitch Control Malfunction, Wind Energy, Power Converters, Power Quality*

Nomenclature

P_{tt}	Mechanical power of the wind turbine.
ρ	Air density.
A	Area covered by the rotor blades.
u	Wind speed value with disturbance.
c_p	Power coefficient.
θ	Pitch angle of the rotor blades.
λ	Tip speed ratio.
P_t	Mechanical power over the rotor of the wind turbine disturbed by the mechanical eigenswings.
A_k	Magnitude of the eigenswing k.
m	Order of the harmonic of an eigenswing.
g_{km}	Distribution of the m-order harmonic in the eigenswing k.
a_{km}	Normalized magnitude of g_{km}.
h_k	Modulation of eigenswing k.
ω_k	Eigenfrequency of the eigenswing k.
φ_{km}	Phase of the m-order harmonic in the eigenswing k.
u_0	Average wind speed.
ω_t	Rotor angular speed at the wind turbine.
J	Moment of inertia for blades, hub and generator of the one-mass model.
T_t	Mechanical torque.
T_g	Electric torque.
J_t	Moment of inertia for blades and hub of the two-mass model.
T_{dt}	Resistant torque in the wind turbine bearing of the two-mass model.
T_{at}	Resistant torque in the hub and blades due to the viscosity of the airflow of the two-mass model.
T_{ts}	Torque of torsional stiffness of the two-mass model.
ω_g	Rotor angular speed at the generator.
J_g	Generator moment of inertia.
T_{dg}	Resistant torque in the generator bearing of the two-mass model.
T_{ag}	Resistant torque due to the viscosity of the airflow in the generator of the two-mass model.
J_b	Moment of inertia of the flexible blades section of the three-mass model.
T_{db}	Resistant torque of the flexible blades of the three-mass model.
T_{bs}	Torsional flexible blades stifness torque of the three-mass model.
ω_h	Rotor angular speed at the rigid blades and the hub of the wind turbine of the three-mass model.
J_h	Moment of inertia of the hub and the rigid blades section of the three-mass model.
T_{dh}	Resistant torque of the rigid blades and the hub of the three-mass model.
T_{ss}	Torsional shaft stifness torque of the three-mass model.
i_f	Equivalent rotor current.
M	Mutual inductance.
p	Number of pairs of poles.
i_d , i_q	Stator currents.

Manuscript received and revised March 2010, accepted April 2010

L_d , L_q	Stator inductances.
R_d , R_q	Stator resistances.
u_d , u_q	Stator voltages.
R_n , L_n	Resistance and the inductance for the model of the electric grid.
i	$i \in \{1,2\}$ in two-level and $i \in \{1,2,3,4\}$ in a multilevel converter identifies a IGBT in a leg.
j	$j \in \{1,2,3\}$ identifies a leg for the rectifier and $j \in \{4,5,6\}$ identifies a leg for the inverter.
u_{fj}	Voltage at the filter.
u_j	Voltage at the electric grid.
S_{ij}	Unidirectional commanded IGBT.
γ_j	Switching variable of the converters used to identify the state of the IGBT in a leg j.
Φ_{1j}	The multilevel converter switching variable for S_{1j} and S_{2j} in leg j.
Φ_{2j}	The multilevel converter switching variable for S_{3j} and S_{4j} in leg j.
v_{dc}	Voltage at the capacitor bank.
v_{C1}	Voltage at the capacitor bank C_1 for the multilevel converter.
v_{C2}	Voltage at the capacitor bank C_2 for the multilevel converter.
${}_aD_t^{\mu}$	Fractional-order differentiator.
μ	Order of derivative or integrals.
$\Re(\mu)$	Real part of the μ.
$\Gamma(x)$	Euler's Gamma function.
!	Factorial operator.
K_p	Proportional constant of the fractional-order PI^{μ} controller.
K_I	Integration constant of the fractional-order PI^{μ} controller.
THD	Total harmonic distortion.
X_H	Root mean square (RMS) value of the total harmonics of the signal.
X_F	RMS value of its fundamental component.

I. Introduction

Electricity restructuring has offered us additional flexibility at both levels of generation and consumption. Also, since restructuring has strike the power system sector, developments in distributed power generation systems (DPGSs) opened new perspectives for electric companies [1]-[2]. DPGSs include, for instance, wind turbines, wave generators, photovoltaic generators, small hydro, and fuel cells. Among DPGSs, the development of wind power generation in recent years is significant, even envisaged as competing with the traditional fossil-fuelled thermal power generation in the near future due to its environmental edge. In Portugal, the wind power goal foreseen for 2010 was established by the government as 3750 MW and that will constitute some 25% of the total installed capacity by 2010 [3]. This value has been raised to 5100 MW, by the most recent governmental goals for the wind sector. Hence, Portugal has one of the most ambitious goals in terms of wind power, and in 2006 was the second country in Europe with the highest wind power growth. Power system stability describes the ability of a power system to maintain synchronism and maintain voltage when subjected to severe transient disturbances [4]. As wind energy is increasingly integrated into power systems, the stability of already existing power systems is becoming a concern of utmost importance [5]. Also, network operators have to ensure that consumer power quality is not compromised. Hence, the THD should be kept as low as possible, improving the quality of the energy injected into the electric grid [6]. The development of power electronics and their applicability in wind energy extraction allowed for variable-speed operation of the wind turbine [7]. The variable-speed wind turbines are implemented with either doubly fed induction generator (DFIG) or full-power converter. In a variable-speed wind turbine with full-power converter, the wind turbine is directly connected to the generator, which is usually a permanent magnet synchronous generator (PMSG). Variable-speed wind turbines usually employ active pitch control, where blade pitch angle increase reduces the captured of wind energy by reducing the angle of attack [8]. The pitch control may have a considerable effect on the dynamical behavior of wind generators. Understanding the harmonic behavior of variable-speed wind turbines is essential in order to analyze their effect on the electric grids where they are connected [9]. Earlier research on simulation of variable-speed wind turbines have mainly focused on problems of harmonic behavior due to external grid faults [8],[10]. Harmonic behavior due to modern variable-speed wind turbines is recognized as having a negative impact on power quality. Therefore, simulations of not only problems due to external grid faults, but also problems due to internal grid faults are necessary for a suitable treatment of the harmonic behavior. This paper focuses on an analysis of wind turbines with PMSG and with a full-power converter subject to a pitch control malfunction, developing stress on the mechanical drive train and consequently affecting the harmonic distortion of the electric current injected into the electric grid. The simulation study is carried out taking into consideration: (i) three different drive train mass models, respectively, one, two and three mass models in order to model the bending flexibility of the blades; (ii) two different topologies for power-electronic converters, respectively a two-level or a multilevel converters; (iii) a fractional-order control strategy, which is compared with a classically used integer-order control strategy.

Simulation results regarding the pitch control malfunction revel that the performance of wind turbines equipped with PMSG and with the two different topologies for the power-electronic converters are improved with the fractional-order control strategy in what regards the (THD) of the electric current injected into the electric grid. This paper is structured as follows. Section 2 presents the modeling for the wind power system with three different drive train mass models, and two different topologies for the power converters, namely two-level and multilevel converters. Section 3 provides the fractional-order control strategy. Section 4 provides the harmonic assessment by the THD. Section 5 presents the simulation. Finally, Section 6 outlines the conclusions.

II. Modeling

II.1. Wind Turbine

The mechanical power of the wind turbine is given by:

$$P_{tt} = \frac{1}{2} \rho A u^3 c_p \tag{1}$$

The power coefficient is a function of the pitch angle of rotor blades, and of the tip speed ratio, which is the ratio between blade tip speed and wind speed value upstream of the rotor. For the simulation of a pitch control malfunction, it is considered that the pitch angle control of the blades imposes momentarily the position of wind gust on the blades, i.e., the blades go to the maximum pitch angle. The maximum pitch angle is 55°, given for the minimum power coefficient, given by:

$$c_{pmin} = 0.0025 \tag{2}$$

for the tip speed ratio given by:

$$\lambda = 3.475 \tag{3}$$

The conversion of wind energy into mechanical energy over the rotor of a wind turbine is influenced by various forces acting on the blades and on the tower of the wind turbine (e.g. centrifugal, gravity and varying aerodynamic forces acting on blades, gyroscopic forces acting on the tower), introducing mechanical effects influencing the energy conversion. Those mechanical effects have been modeled by eigenswings mainly due to the following phenomena: asymmetry in the turbine, vortex tower interaction, and eigenswing in the blades. The mechanical power over the rotor of the wind turbine has been modeled, using the mechanical eigenswings, as a set of harmonic terms multiplied by the power associated with the energy capture from the wind by the blades. The mechanical power over the rotor of the wind turbine has been modeled, using the mechanical eigenswings, as a set of harmonic terms multiplied by the power associated with the energy capture from the wind by the blades. In this paper, the model developed in [11]-[12] is followed, where the mechanical power over the rotor of the wind turbine disturbed by the mechanical eigenswings is given by:

$$P_t = P_{tt} \left[1 + \sum_{k=1}^{3} A_k \left(\sum_{m=1}^{2} a_{km}\, g_{km}(t) \right) h_k(t) \right] \tag{4}$$

$$g_{km} = sin\left(\int_0^t m\, \omega_k(t')\, dt' + \varphi_{km} \right) \tag{5}$$

The frequency range of the wind turbine model with mechanical eigenswings is from 0.1 to 10 Hz. The values used for computing (4) and (5) are given in Table I [12].

TABLE I
MECHANICAL EIGENSWINGS EXCITED IN THE WIND TURBINE

n	Source	A_n	ω_n	h_n	m	a_{nm}	φ_{nm}
1	Asymmetry	0.01	ω_t	1	1	4/5	0
					2	1/5	π/2
2	Vortex tower interaction	0.08	3 ω_t	1	1	1/2	0
					2	1/2	π/2
3	Blades	0.15	9 π	1/2 (g_{11}+g_{21})	1	1	0

II.2. Wind Speed

The wind speed usually varies considerably and has a stochastic character. The wind speed variation can be modeled as a sum of harmonics with frequency range 0.1–10 Hz [11]:

$$u = u_0 \left[1 + \sum_k A_k\, sin(\omega_k\, t) \right] \tag{6}$$

The values used for the calculation of u are given in Table I [12]. Hence, the physical wind turbine model is subjected to the disturbance given by the wind speed variation model [12].

II.3. One-Mass Drive Train

In a one-mass drive train model, all components are lumped together and modeled as a single rotating mass [13]. The equation for the one-mass model is based on the second law of Newton, deriving the state equation for the rotor angular speed at the wind turbine, given by [12]:

$$\frac{d\omega_t}{dt} = \frac{1}{J} \left(T_t - T_g \right) \tag{7}$$

II.4. Two-Mass Drive Train

A comparative study of wind turbine generator system using different drive train models [14] has shown that the two-mass model may be more suitable for transient stability analysis.

The equations for the two-mass model are based on the torsional version of the second law of Newton, deriving the state equation for the rotor angular speed at the wind turbine and for the rotor angular speed at the generator, respectively given by:

$$\frac{d\omega_t}{dt} = \frac{1}{J_t}\left(T_t - T_{dt} - T_{at} - T_{ts}\right) \tag{8}$$

$$\frac{d\omega_g}{dt} = \frac{1}{J_g}\left(T_{ts} - T_{dg} - T_{ag} - T_g\right) \tag{9}$$

II.5. Three-Mass Drive Train

With the increase in size of the wind turbines, one question arises whether long flexible blades have an important impact on the transient stability analysis of wind energy systems during a fault [15]. To determine the dynamic properties of the blade, finite element techniques may be used but this approach cannot easily be implemented in power systems analysis programs.

Hence, to avoid the use of the finite element approach it is necessary to simplify the rotor dynamics as much as possible. One way to achieve this is represented in Fig. 1, where the blade analysis is represented as a simple torsional system. Since the blade bending occurs at a significant distance from the joint between the blade and the hub, the blade can be split in two parts, OA and AB.

The blade sections OA1, OA2 and OA3 has the moment of inertia of the hub and the rigid blade sections of the three-mass model, the rest of the blade sections A1B1, A2B2 and A3B3 is the effective flexible blade sections and it has the moment of inertia of the flexible blade sections of the three-mass model [16].

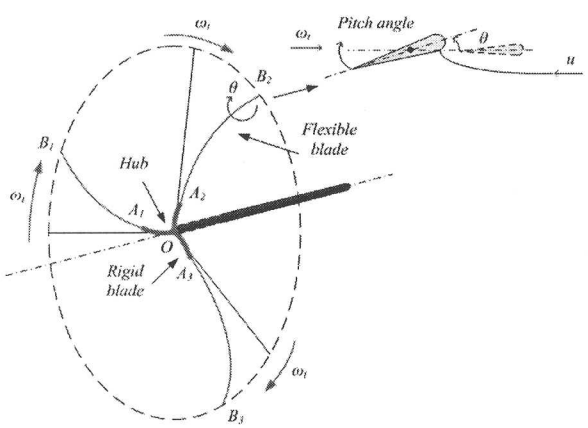

Fig. 1. Blade bending dynamics for the three-mass drive train model

The configuration of the three-mass drive train model is shown in Fig. 2.

The mass moments of inertia for the model are given as input data, but in their absence an estimation of the mass moments of inertia is possible.

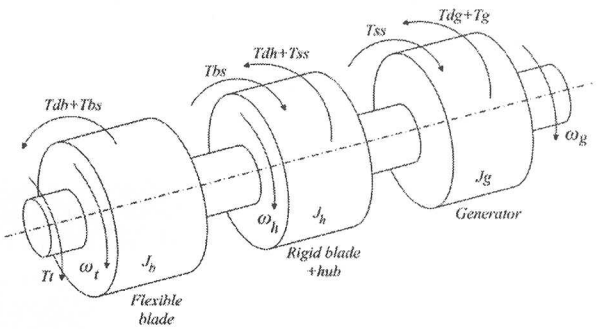

Fig. 2. Configuration of the three-mass drive train model

The equations for the three-mass model are based on the torsional version of the second law of Newton, deriving the state equation for the rotor angular speed at the wind turbine and for the rotor angular speed at the generator, respectively given by:

$$\frac{d\omega_t}{dt} = \frac{1}{J_b}\left(T_t - T_{db} - T_{bs}\right) \tag{10}$$

$$\frac{d\omega_h}{dt} = \frac{1}{J_h}\left(T_{bs} - T_{dh} - T_{ss}\right) \tag{11}$$

$$\frac{d\omega_g}{dt} = \frac{1}{J_g}\left(T_{ss} - T_{dg} - T_g\right) \tag{12}$$

II.6. Generator

The generator considered in this paper is a PMSG. The equations for modeling a PMSG can be found in the literature [17]. Using the motor machine convention, the equations are considered:

$$\frac{di_d}{dt} = \frac{1}{L_d}\left[u_d + p\omega_g L_q i_q - R_d i_d\right] \tag{13}$$

$$\frac{di_q}{dt} = \frac{1}{L_q}\left[u_q - p\omega_g\left(L_d i_d + M i_f\right) - R_q i_q\right] \tag{14}$$

The electric power P_g is given by:

$$P_g = \left[u_d \quad u_q \quad u_f\right]\left[i_d \quad i_q \quad i_f\right]^T \tag{15}$$

In order to avoid demagnetization of permanent magnet in the PMSG, a null stator current associated with de direct axis is imposed [18].

II.7. Two-Level Converter

The two-level converter is an AC/DC/AC converter, with six unidirectional commanded insulated gate bipolar transistors (IGBTs) used as a rectifier, and with the same number of unidirectional commanded IGBTs used as an inverter. The rectifier is connected between the PMSG

and a capacitor bank. The inverter is connected between this capacitor bank and a second order filter, which in turn is connected to an electric grid. The configuration of the simulated wind power system with two-level converter is shown in Fig. 3. The two conditions [19]-[20] for the switching variable of each leg j are given by:

$$\gamma_j = \begin{cases} 1, & (S_{1j} = 1 \text{ and } S_{2j} = 0) \\ 0, & (S_{1j} = 0 \text{ and } S_{2j} = 1) \end{cases} \quad j \in \{1, \ldots, 6\} \tag{16}$$

The topological restriction for the leg j is given by:

$$\sum_{i=1}^{2} S_{ij} = 1 \qquad j \in \{1, \ldots, 6\} \tag{17}$$

Each switching variable depends on the conduction and blockade states of the IGBTs. The voltage at the capacitor bank is modeled by a state equation, given by:

$$\frac{dv_{dc}}{dt} = \frac{1}{C}\left(\sum_{j=1}^{3} \gamma_j i_j - \sum_{j=4}^{6} \gamma_j i_j\right) \tag{18}$$

II.8. Multilevel Converter

The multilevel converter is an AC/DC/AC converter, with twelve unidirectional commanded IGBTs used as a rectifier, and with the same number of unidirectional commanded IGBTs used as an inverter. The rectifier is connected between the PMSG and a capacitor bank. The inverter is connected between this capacitor bank and a second order filter, which in turn is connected to an electric grid. The groups of four IGBTs linked to the same phase constitute a leg of the converter. The configuration of the simulated wind power system with multilevel converter is shown in Fig. 4. The three valid conditions [19]-[20] for the switching variable of each leg j are given by:

$$\gamma_j = \begin{cases} 1, & (S_{1j} \text{ and } S_{2j}) = 1 \text{ and } (S_{3j} \text{ or } S_{4j}) = 0 \\ 0, & (S_{2j} \text{ and } S_{3j}) = 1 \text{ and } (S_{1j} \text{ or } S_{4j}) = 0 \\ -1, & (S_{3j} \text{ and } S_{4j}) = 1 \text{ and } (S_{1j} \text{ or } S_{2j}) = 0 \end{cases}$$
$$j \in \{1, \ldots, 6\} \tag{19}$$

The topological restriction for the leg is given by:

$$(S_{1j}.S_{2j}) + (S_{2j}.S_{3j}) + (S_{3j}.S_{4j}) = 1 \quad j \in \{1, \ldots, 6\} \tag{20}$$

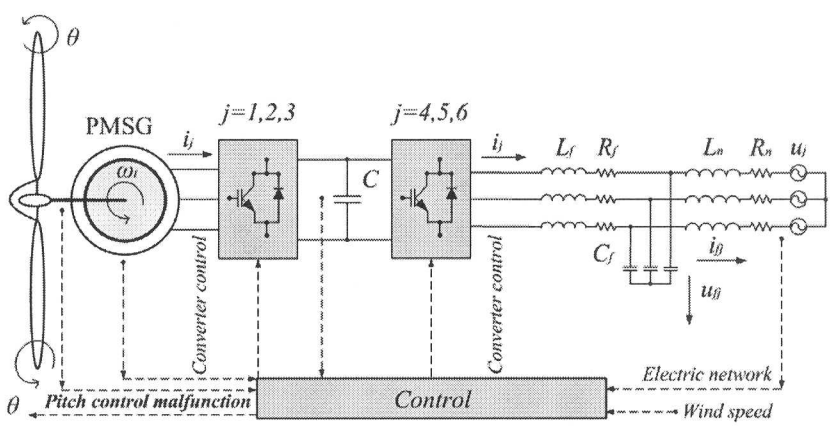

Fig. 3. Wind power system with two-level converter

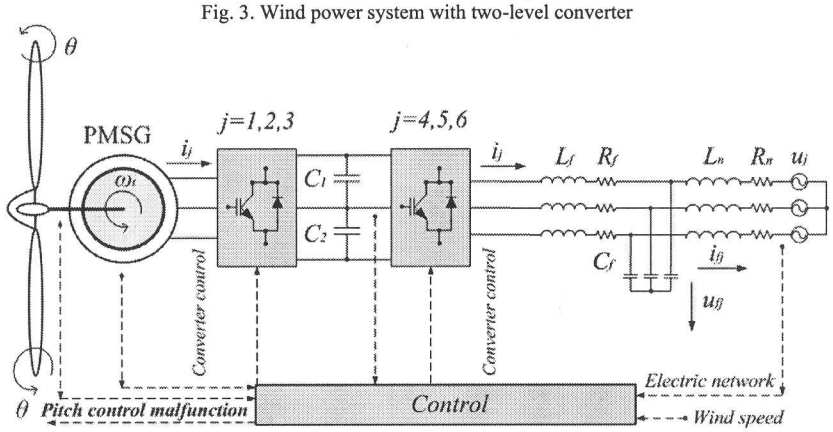

Fig. 4. Wind power system with multilevel converter

The switching variables for the uppers and lowers IGBTs are respectively given by:

$$\Phi_{1j}=\frac{\gamma_j\left(1+\gamma_j\right)}{2} \quad \Phi_{2j}=\frac{\gamma_j\left(1-\gamma_j\right)}{2} \quad j\in\{1,\ldots,6\} \quad (21)$$

Each switching variable depends on the conduction and blockade states of the IGBTs.

The total voltage at the capacitor bank is the sum of the two voltages at capacitor banks C_1 and C_2, and is modeled by a state equation, given by:

$$\frac{dv_{dc}}{dt}=\frac{1}{C_1}\left(\sum_{j=1}^{3}\Phi_{1j}i_j-\sum_{j=4}^{6}\Phi_{1j}i_j\right)+ +\frac{1}{C_2}\left(\sum_{j=1}^{3}\Phi_{2j}i_j-\sum_{j=4}^{6}\Phi_{2j}i_j\right) \quad (22)$$

II.9. Electric Grid

A three-phase active symmetrical circuit in series models the electric grid [19]-[20]. The phase currents injected in the electric network are modeled by the state equation given by:

$$\frac{di_{fj}}{dt}=\frac{1}{L_n}\left(u_{fj}-R_n\,i_{fj}-u_j\right) \quad j=\{4,5,6\} \quad (23)$$

III. Control Strategy

III.1. Fractional-Order Controller

Fractional-order calculus used in mathematical models of the systems is known by some propensity to improve the design properties and control abilities in dynamical systems [21].

Although, the design of fractional-order controls are more complex than that of classical PI controllers [22], fractional-order controls are one option that has been considered in order to eventually improve the behavior of systems. A control strategy based on fractional-order PI^{μ} controllers is studied for the variable-speed operation of wind turbines with PMSG/full-power converters in this paper.

Fractional calculus theory is a generalization of ordinary differentiation and integration to arbitrary (non-integer) order [23]. The fractional-order differentiator is given by [24]:

$${}_aD_t^{\mu}=\begin{cases}\dfrac{d^{\mu}}{dt^{\mu}}, & \Re(\mu)>0\\ 1, & \Re(\mu)=0\\ \int_a^t(d\tau)^{-\mu}, & \Re(\mu)<0\end{cases} \quad (24)$$

The mathematical definition of fractional derivative and integral has been the subject of several descriptions. The most frequently encountered one is called Riemann–Liouville definition, in which the fractional-order integral is given by [25]:

$${}_aD_t^{-\mu}\,f(t)=\frac{1}{\Gamma(\mu)}\int_a^t(t-\tau)^{\mu-1}f(\tau)\,d\tau \quad (25)$$

while the definition of fractional-order derivative is:

$${}_aD_t^{\mu}\,f(t)=\frac{1}{\Gamma(n-\mu)}\frac{d^n}{dt^n}\left[\int_a^t\frac{f(\tau)}{(t-\tau)^{\mu-n+1}}\,d\tau\right] \quad (26)$$

where a and t are the limits of the operation and the Euler's Gamma function is given by:

$$\Gamma(x)\equiv\int_0^{\infty}y^{x-1}\,e^{-y}\,dy \quad (27)$$

In this paper, μ is assumed as a real number that satisfies the restrictions $0<\mu<1$. Also, it is assumed that $a=0$. The following convention is used: ${}_0D_t^{-\mu}\equiv D_t^{-\mu}$.

The other approach is Grünwald–Letnikov definition of fractional-order integral, given by:

$${}_aD_t^{-\mu}\,f(t)=\lim_{h\to0}h^{\mu}\sum_{r=0}^{\frac{t-a}{h}}\frac{\Gamma(\mu+r)}{r!\Gamma(\mu)}f(t-rh) \quad (28)$$

while the definition of fractional-order derivative is given by:

$${}_aD_t^{\mu}\,f(t)= =\lim_{h\to0}h^{-\mu}\sum_{r=0}^{\frac{t-a}{h}}(-1)^r\frac{\Gamma(\mu+1)}{r!\Gamma(\mu-r+1)}f(t-rh) \quad (29)$$

An important property revealed by the Riemann–Liouville and Grünwald–Letnikov definitions is that while integer-order operators imply finite series, the fractional-order counterparts are defined by infinite series [21]-[24]. This means that integer operators are local operators in opposition with the fractional operators that have, implicitly, a memory of the past events.

The differential equation of the fractional-order PI^{μ} $0<\mu<1$ controller is given by:

$$u(t)=K_p\,e(t)+K_I\,D_t^{-\mu}\,e(t) \quad (30)$$

Taking $\mu=1$, a classical PI controller is obtained. The fractional-order PI^{μ} controller is more flexible than the classical PI controller, because it has one more adjustable parameter, which can reflect the intensity of

integration [26]. The transfer function of the fractional-order PI^{μ} controller, using the Laplace transform on (30), is given by:

$$G(s)=K_p+K_I\,s^{-\mu} \tag{31}$$

III.2. Converters Control

Power converters are variable structure systems, because of the on/off switching of their IGBTs. As mentioned previously, the controllers used in the converters are fractional-order PI^{μ} controllers. Pulse width modulation (PWM) by space vector modulation (SVM) associated with sliding mode is used for controlling the converters.

The sliding mode control strategy presents attractive features such as robustness to parametric uncertainties of the wind turbine and the generator as well as to electric grid disturbances [27].

Sliding mode controllers are particularly interesting in systems with variable structure, such as switching power converters, guaranteeing the choice of the most appropriate space vectors. Their aim is to let the system slide along a predefined sliding surface by changing the system structure. The power semiconductors present physical limitations that have to be considered during design phase and during performance simulation. Particularly, they cannot switch at infinite frequency. Also, for a finite value of the switching frequency, an error $e_{\alpha\beta}$ will exist between the reference value and the control value. In order to guarantee that the system slides along the sliding surface $S(e_{\alpha\beta},t)$, it has been proven that it is necessary to ensure that the state trajectory near the surfaces verifies the stability conditions [19]-[20] given by:

$$S\left(e_{\alpha\beta},t\right)\frac{dS\left(e_{\alpha\beta},t\right)}{dt}<0 \tag{32}$$

in practice a small error $\varepsilon>0$ for $S(e_{\alpha\beta},t)$ is allowed, due to power semiconductors switching only at finite frequency. Consequently, a switching strategy has to be considered, given by:

$$-\varepsilon<S\left(e_{\alpha\beta},t\right)<+\varepsilon \tag{33}$$

At the simulation level, a practical implementation of the switching strategy considered in Eq. (33) could be accomplished by using hysteresis comparators.

The outputs of the hysteresis comparators are the integer variables $\sigma_{\alpha\beta}=\left(\sigma_\alpha,\sigma_\beta\right)$ [19]-[20]. For the two-level converter, σ_α and σ_β assume values in the set Ω given by:

$$\Omega\in\{-1,0,1\} \tag{34}$$

The appropriate vector selection in order to ensure stability for the two-level converter is shown in Table II.

TABLE II
OUTPUT VOLTAGE VECTORS SELECTION FOR THE TWO-LEVEL CONVERTER

$\sigma_\beta \backslash \sigma_\alpha$	-1	0	1
-1	4	4;5	5
0	6	0;7	1
1	2	3;2	3

The output voltage vectors in the $\alpha\beta$ plane for the two-level converter are shown in Fig. 5.

For the multilevel converter, σ_α and σ_β assume values in the set Ω given by:

$$\Omega\in\{-2,-1,0,1,2\} \tag{35}$$

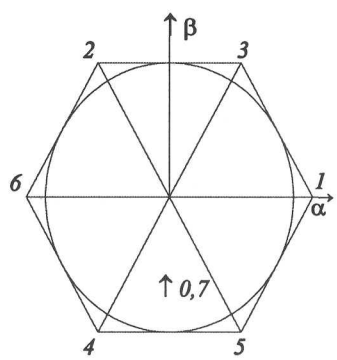

Fig. 5. Output voltage vectors for the two-level converter

The output voltage vectors in the $\alpha\beta$ plane for the multilevel converter are shown in Fig. 6.

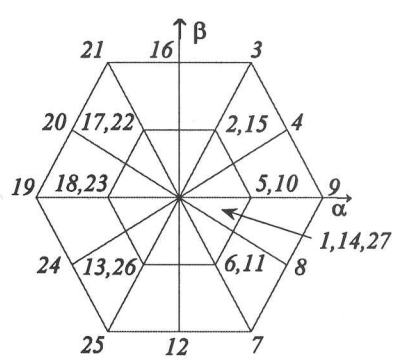

Fig. 6. Output voltage vectors for the multilevel converter

In this control strategy, only when $v_{C1}\neq v_{C2}$ a new vector is selected. The appropriate vector selection in order to ensure stability for the multilevel converter is shown in Table III, for $v_{C1}>v_{C2}$, and in Table IV, for $v_{C1}<v_{C2}$.

TABLE III
OUTPUT VOLTAGE VECTORS SELECTION FOR THE MULTILEVEL CONVERTER FOR $v_{C1} > v_{C2}$

$\sigma_\beta \setminus \sigma_\alpha$	-2	-1	0	1	2
-2	25	25	12	7	7
-1	24	13	13;6	6	8
0	19	18	1;14;27	5	9
1	20	17	17;2	2	4
2	21	21	16	3	3

TABLE IV
OUTPUT VOLTAGE VECTORS SELECTION FOR THE MULTILEVEL CONVERTER FOR $v_{C1} < v_{C2}$

$\sigma_\beta \setminus \sigma_\alpha$	-2	-1	0	1	2
-2	25	25	12	7	7
-1	24	26	26;11	11	8
0	19	23	1;14;27	10	9
1	20	22	22;15	15	4
2	21	21	16	3	3

IV. Harmonic Assessment

In order to evaluate the harmonic content of the current injected in the electrical grid, the THD is used. The harmonic content of the current is expressed in percentage of the fundamental component. The THD is given by:

$$\mathrm{THD}\,(\%) = 100\,\frac{\sqrt{\sum_{H=2}^{50} X_H^2}}{X_F} \tag{36}$$

V. Simulation

The mathematical models for the wind power system with the two-level and multilevel converters were implemented in Matlab/Simulink. The wind power system simulated has a rated electric power of 900 kW.

The time horizon considered in the simulation is 5 s. For the fractional-order PI^{μ} controllers a good tradeoff, presented in [28], between robustness and dynamic performance is in favour of the range $0.4 \le \mu \le 0.6$ for the order of integration. Hence, in this paper after some tuning it is assumed $\mu = 0.5$. The wind speed model considered in this paper is given by:

$$u(t) = 15\left[1 + \sum_k A_k \sin(\omega_k t)\right] \quad 0 \le t \le 5 \tag{37}$$

Fig. 7 shows the profile of the wind speed.

A pitch control malfunction is simulated between 2 and 2.5 s, imposing a total cut-off on the capture of the energy from the wind by the blades.

Fig. 8 shows the mechanical power over the rotor of the wind turbine disturbed by the mechanical eigenswings, and the electric power of the generator.

The pitch angle behavior is shown in Fig. 9. The pitch angle is at 55° during pitch control malfunction, corresponding to the position of wind gust on the blades.

The power coefficient behavior is shown in Fig. 10. The power coefficient is at zero value during pitch control malfunction.

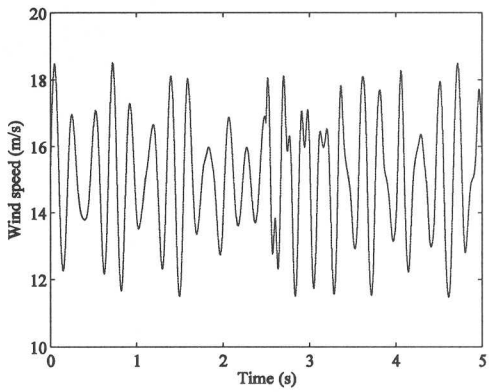

Fig. 7. Profile of the wind speed

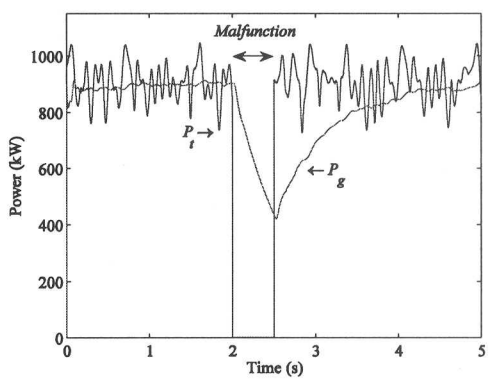

Fig. 8. Mechanical power over the rotor and electric power

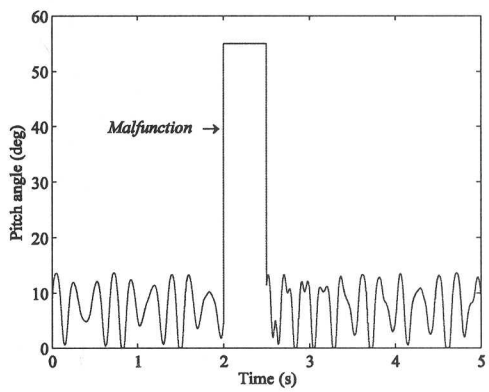

Fig. 9. Pitch angle variation

In order to access the models ability to predict the behavior for the drive train, the rotor speeds at the

generator considering respectively the three different mass drive train models are shown in Fig. 11. The voltage v_{dc} for the two-level converter with a $PI^{0.5}$ controller, for the three different mass drive train models are shown in Fig. 12.

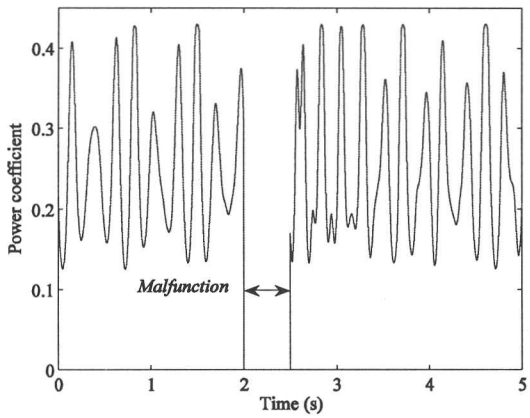

Fig. 10. Power coefficient variation

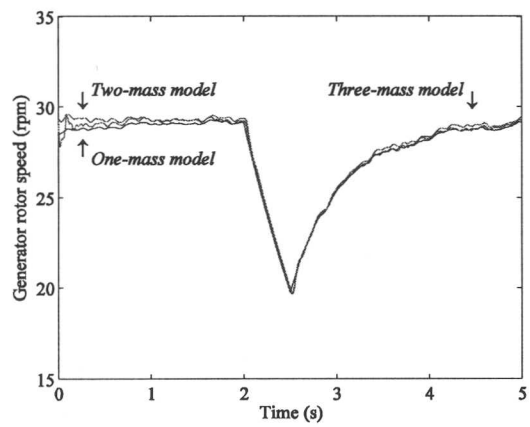

Fig. 11. Rotor speeds at the generator with the three different mass drive train models

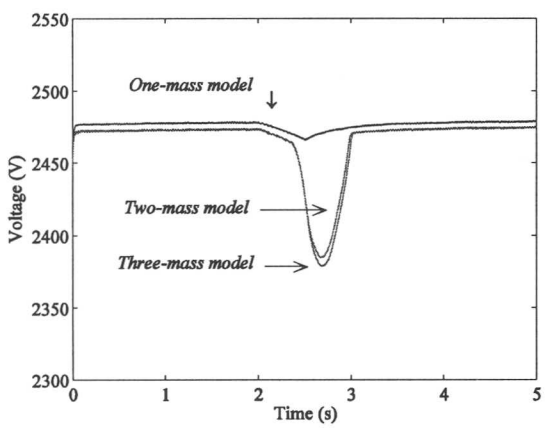

Fig. 12. Voltage v_{dc} for the two-level converter considering the fractional-order controller

The voltage v_{dc} for the multilevel converter with a $PI^{0.5}$ controller, for the three different mass drive train models are shown in Fig. 13.

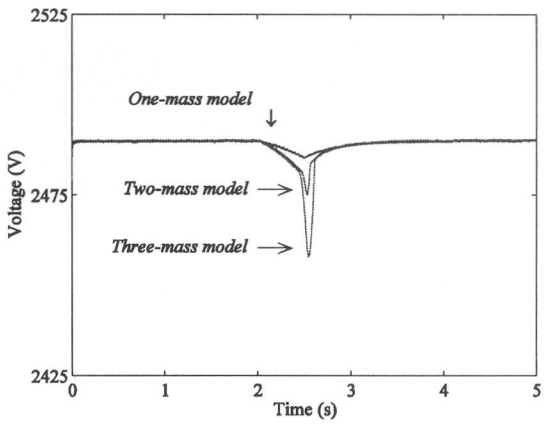

Fig. 13. Voltage v_{dc} for the multilevel converter considering the fractional-order controller

The assessment of the models ability to predict the behavior for the drive train is in favor of the three-mass model, since it renders a dynamic behavior for the drive train. Fig. 12 and Fig. 13 reveal the reality of a larger drop on the DC voltage at the converter, during pitch control malfunction, in comparison with the one-mass model drive train and the two-mass model drive train. The voltage drops are always inferior for the multilevel converter, in comparison with the ones for the two-level converter. A comparison between the maximum values for the DC voltage drops for the two-level converter is shown in Table V.

TABLE V
CAPACITOR VOLTAGE DROP DURING CONTROL MALFUNCTION FOR THE WIND POWER SYSTEM WITH TWO-LEVEL CONVERTER

Controller	v_{dc} (V)	
	Classical PI	Fractional $PI^{0.5}$
One-mass model	19	12
Two-mass model	100	91
Three-mass model	110	101

A comparison between the maximum values for the DC voltage drops for the multilevel converter is shown in Table VI. The voltage v_{dc} drops only 33 V during the pitch control malfunction with the three-mass model drive train for the multilevel converter and the fractional $PI^{0.5}$ controller. While, the voltage v_{dc} drops almost 110 V during the pitch control malfunction with the three-mass model drive train, the two-level converter and the classical PI controller. This is the worst voltage v_{dc} drop case.

TABLE VI
CAPACITOR VOLTAGE DROP DURING CONTROL MALFUNCTION FOR THE WIND POWER SYSTEM WITH MULTILEVEL CONVERTER

Controller	v_{dc} (V)	
	Classical PI	Fractional $PI^{0.5}$
One-mass model	9	5
Two-mass model	21	16
Three-mass model	42	33

The current injected in the electric grid with the fractional-order controller for the two-level converter is shown in Fig. 14 and the one for the multilevel converter is shown in Fig. 15.

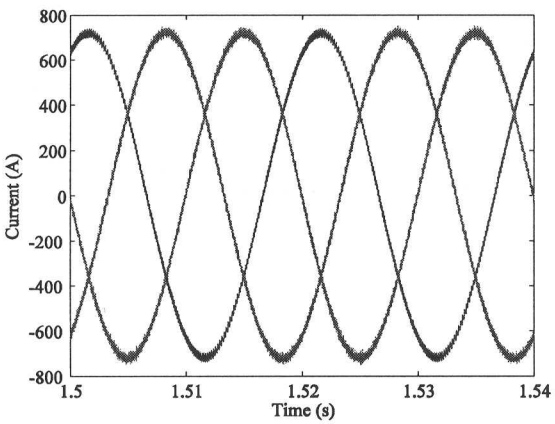

Fig. 14. Current injected in the electric grid for the two-level converter

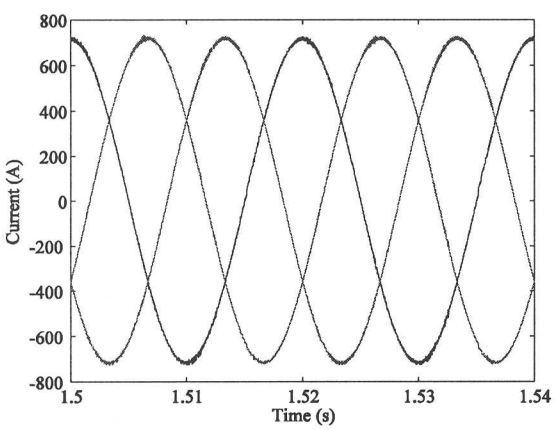

Fig. 15. Current injected in the electric grid for the multilevel converter

The THD of the current injected in the electric grid considering the three-mass model drive train with the fractional-order controller and a two-level converter is shown in Fig. 16, while the one with the multilevel converter is shown in Fig. 17.

Table VII summarizes a comparison between the control strategies in what regards the THD for the wind power system with two-level converter.

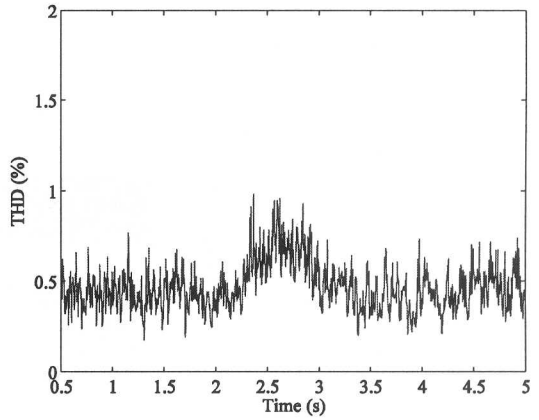

Fig. 16. THD of the current injected in the electric grid with the two-level converter

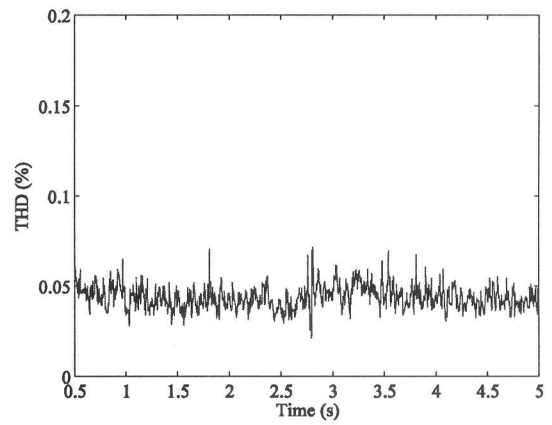

Fig. 17. THD of the current injected in the electric grid with the multilevel converter

TABLE VII
THD OF THE CURRENT INJECTED IN THE ELECTRIC GRID FOR THE WIND POWER SYSTEM WITH TWO-LEVEL CONVERTER

Controller	THD (%)	
	Classical PI	Fractional $PI^{0.5}$
One-mass model	0.40	0.26
Two-mass model	0.46	0.29
Three-mass model	0.51	0.33

Table VIII summarizes a comparison between the control strategies in what regards the THD for the wind power system with multilevel converter.

The control strategy, based on fractional-order controllers, improves the performance in comparison with the classical PI control strategy. Moreover, the quality of the energy injected into the electric grid is improved in what regards the THD at a lower level.

Accordingly, it is shown that the current THD for the wind power system with either a two-level or a multilevel converter is lower than 5% limit imposed by IEEE-519 standard [29].

Although IEEE-519 standard might not be applicable

in such situation, it is used as a guideline for comparison purposes [30].

TABLE VIII
THD OF THE CURRENT INJECTED IN THE ELECTRIC GRID FOR THE WIND POWER SYSTEM WITH MULTILEVEL CONVERTER

Controller	THD (%)	
	Classical PI	Fractional $PI^{0.5}$
One-mass model	0.06	0.03
Two-mass model	0.08	0.05
Three-mass model	0.11	0.07

VI. Conclusion

The increased wind power penetration leads to new technical challenges, transient stability and power quality. In this paper, simulations studies for variable speed wind turbines equipped with a PMSG and two different topologies for the power-electronic converters are carried out. The studied fractional-order controller for the variable-speed operation of wind turbines equipped with a PMSG and multilevel converter improves the power quality in comparison with a classical integer-order control strategy, in what regards the THD. Accordingly, it is show that the current THD for the wind power system with either a two-level or a multilevel converter is lower than 5% limit imposed by IEEE-519 standard. Also, the assessment of the models ability to predict the behavior for the drive train is in favor of the three-mass model. A more systematic procedure for controllers design needs further research in order to well develop tuning implementation techniques for an easygoing design of fractional-order controllers.

References

[1] M. Mashhour, M. A. Golkar, S. M. Moghaddas Tafreshi, Aggregated model of distribution network with distributed resources, *International Review of Electrical Engineering-IREE, vol. 4 n. 4*, 2009, pp. 583-591.

[2] J.A. Peças Lopes, N. Hatziargyriou, J. Mutale, P. Djapic, N. Jenkins, Integrating distributed generation into electric power systems: A review of drivers, challenges and opportunities, *Electr. Power Syst. Res, vol. 77 n. 9*, 2007, pp. 1189 – 1203.

[3] A. Estanqueiro, R. Castro, P. Flores, J. Ricardo, M. Pinto, R. Rodrigues, J. Peças Lopes, How to prepare a power system for 15% wind energy penetration: the Portuguese case study, *Wind Energy, vol. 11 n. 1*, 2008, pp. 75 – 84.

[4] Y. Coughlan, P. Smith, A. Mullane, M. O'Malley, Wind turbine modelling for power system stability analysis - A system operator perspective, *IEEE Trans. Power Syst, vol. 22 n. 3*, 2007, pp. 929 – 936.

[5] N.R. Ullah, T. Thiringer, Variable speed wind turbines for power system stability enhancement, *IEEE Trans. Energy Convers, vol. 22 n. 1*, 2007, pp. 52 – 60.

[6] J.M. Carrasco, L.G. Franquelo, J.T. Bialasiewicz, E. Galvan, R.C.P. Guisado, A.M. Prats, J.I. Leon, N. Moreno-Alfonso, Power-electronic systems for the grid integration of renewable energy sources: A survey, *IEEE Trans. Ind. Electron, vol. 53 n. 4*, 2006, pp. 1002 – 1016.

[7] J.A. Baroudi, V. Dinavahi, A.M. Knight, A review of power converter topologies for wind generators, *Renew. Energy, vol. 32 n. 14*, 2007, pp. 2369 – 2385.

[8] J.F. Conroy, R. Watson, Low-voltage ride-through of a full converter wind turbine with permanent magnet generator, *IET Renew. Power Gener, vol. 1 n. 3*, 2007, pp. 182 – 189.

[9] S.T. Tentzrakis, S. A. Papathanassiou, An investigation of the harmonic emissions of wind turbines, *IEEE Trans. Energy Convers, vol. 22 n. 1*, 2007, pp. 150 – 158.

[10] C. Jauch, Transient and dynamic control of a variable speed wind turbine with synchronous generator, *Wind Energy, vol. 10 n. 3*, 2007, pp. 247 – 269.

[11] Z.X. Xing, Q.L. Zheng, X.J. Yao, Y.J. Jing, Integration of large doubly-fed wind power generator system into grid, *The 8th Int. Conference Electrical Machines and Systems 2005*, pp. 1000 – 1004, 2005, Nanjing, China Nanjing, China.

[12] V. Akhmatov, H. Knudsen, A.H. Nielsen, Advanced simulation of windmills in the electric power supply, *Int. J. Electr. Power Energy Syst, vol. 22 n. 6*, 2000, pp. 421 – 434.

[13] S.K. Salman, A. L. J. Teo, Windmill modeling consideration and factors influencing the stability of a grid-connected wind power-based embedded generator, *IEEE Trans. Power Syst, vol. 18*, 2003, pp. 793 – 802.

[14] S.M. Muyeen, M. Hassan Ali, R. Takahashi, T. Murata, J. Tamura, Y. Tomaki, A. Sakahara, E. Sasano, Transient stability analysis of grid connected wind turbine generator system considering multi-mass shaft modeling, *Electr. Power Compon. Syst, vol. 34*, 2006, pp. 1121 – 1138.

[15] H. Li, Z. Chen, Transient stability analysis of wind turbines with induction generators considering blades and shaft flexibility, *The 33rd IEEE IECON 2007*, pp. 1604 – 1609, 2007, Taipei, Taiwan.

[16] G. Ramtharan, N. Jenkins, Influence of rotor structural dynamics representations on the electrical transient performance of DFIG wind turbines, *Wind Energy, vol. 10*, 2007, pp. 293 – 301.

[17] C.-M. Ong, Dynamic Simulation of Electric Machinery: Using Matlab/Simulink, (New Jersey: Prentice-Hall, 1998, 259 – 350).

[18] T. Senjyu, S. Tamaki, N. Urasaki, K. Uezato, Wind velocity and position sensorless operation for PMSG wind generator, *The 5th Int. Conference on Power Electronics and Drive Systems 2003*, pp. 787 – 792, 2003, Singapore.

[19] R. Melício, V.M.F. Mendes, J.P.S. Catalão, Two-level and multilevel converters for wind energy systems: a comparative study, *The 13th Int. Power Electronics and Motion Control Conference ~EPE-PEMC 2008~*, pp. 1682 – 1687, 2008, Poznań, Poland.

[20] R. Melício, V.M.F. Mendes, J.P.S. Catalão, Evaluating power quality in wind power generation systems with two-level and multi-level converters, *The 6th Mediterranean Conference and Exhibition on Power Generation, Transmission And Distribution ~MEDPOWER 2008~*, 2008, Thessaloniki, Greece.

[21] C. Jun-Yi, C. Bing-Gang, Design of fractional order controllers based on particle swarm optimization, *The IEEE ICIEA 2006*, pp. 1 – 6, 2006, Singapore.

[22] B. Arijit, D. Swagatam, A. Ajith, D. Sambarta, Design of fractional-order PI-lambda-D-mu-controllers with an improved differential evolution, *Eng. Appl. Artif. Intell, vol. 22*, 2009, pp. 343 – 350.

[23] I. Podlubny, Fractional-order systems and PI-lambda-D-mu-controllers, *IEEE Trans. Autom. Control, vol. 44 n. 1*, 1999, pp. 208 – 214.

[24] A.J. Calderón, B.M. Vinagre, V. Feliu, Fractional order control strategies for power electronic buck converters, *Signal Process, vol. 86 n. 10*, 2006, pp. 2803 – 2819.

[25] C. Ma, Y. Hori, Fractional order control and its application of (PID)-D-alpha controller for robust two-inertia speed control, *The 4th Int. Power Electronics and Motion Control Conference ~ EPE-PEMC 2004~*, pp. 1477 – 1482, 2004, Xian, China.

[26] K. Zong, S. Li, X. Lin, The application of fractional-order PI control algorithm to the PMSM speed-adjusting system, *The 3rd Int. Conf. on Intelligent Computing 2007*, pp. 660 – 669, 2007, Qingdao, China.

[27] B. Beltran, T. Ahmed-Ali, M. E. H. Benbouzid, Sliding mode power control of variable-speed wind energy conversion system, *IEEE Trans. Energy Convers, vol. 23 n. 2*, 2008, pp. 551 – 558.

[28] G. Maione and P. Lino, New tuning rules for fractional PI-alfa controllers, *Nonlinear Dynamics, vol. 49 n. 1-2*, 2007, pp. 251 – 257.
[29] IEEE Guide for Harmonic Control and Reactive Compensation of Static Power Converters, IEEE Standard 519-1992.
[30] T.M.H. Nicky, K. Tan, S. Islam, Mitigation of harmonics in wind turbine driven variable speed permanent magnet synchronous generators, *The 7th Int. Power Engineering Conf 2005*, pp. 1159 – 1164, 2005, Singapore.

Authors' information

[1]University of Beira Interior. catalao@ubi.pt

[2]Instituto Superior de Engenharia de Lisboa.

R. Melício was born in Lisbon, Portugal, May 1954. He received the M.Sc. degree from the Instituto Superior Técnico, Lisbon, Portugal, in 2004.
He is currently a Ph.D. student at the University of Beira Interior, in collaboration with the Instituto Superior de Engenharia de Lisboa, Lisbon, Portugal. His research interests include power electronic converters, power quality, and wind energy systems.

V. M. F. Mendes was born in Lisbon, Portugal, January 1954. He received the M.Sc. and Ph.D. degrees from the Instituto Superior Técnico, Lisbon, Portugal, in 1987 and 1994, respectively.
He is currently a Coordinator Professor with Aggregation at the Instituto Superior de Engenharia de Lisboa, Lisbon, Portugal. His research interests include hydrothermal scheduling, optimization theory and its applications, and renewable energies.

J. P. S. Catalão was born in Covilha, Portugal, January 1976. He received the M.Sc. degree from the Instituto Superior Técnico, Lisbon, Portugal, in 2003 and the Ph.D. degree from the University of Beira Interior, Covilha, Portugal, in 2007.
He is currently an Assistant Professor at the University of Beira Interior. His research interests include hydro scheduling, unit commitment, price forecasting, wind energy systems, and electricity markets. He has authored or coauthored more than 110 technical papers. Also, he is an Associate Editor for the International Journal of Power and Energy Systems, and a Member of the Editorial Board of Electric Power Components & Systems.